FUDMA Journal of Sciences (FJS)
ISSN online: 2616-1370
ISSN print: 2645 - 2944
Vol. 10 No. 24, December (Special Issue), 2026, pp 137 – 142
DOI: https://doi.org/10.33003/fjs-2026-1024SI-6628

Design, Optimization and Experimental Characterization of a Compact Ultra-Wideband Monopole Antenna for Biomedical Imaging Applications

[*1]Isah Musa Danjuma, [2]Salamatu Abubakar Ibrahim and [2]Raed Abd Alhameed

[1]Department of Electrical Engineering, Nigerian Defence Academy, Kaduna State, Nigeria.
[2]Department of Electrical Engineering, University of Bradford, Bradford, United Kingdom.

*Corresponding authors' email: imdanjuma@nda.edu.ng

Received: 05 Nov. 2026
Accepted: 24 Nov. 2026
Published: 28 Nov. 2026

ABSTRACT
This study presents the design, optimisation, fabrication and experimental characterisation of a compact slotted ultra-wideband (UWB) monopole antenna for potential biomedical imaging applications. The radiating element is a circular patch incorporating four interconnected T-shaped slots that converge towards the centre to form a quasi-cross configuration. The antenna is fabricated on an FR-4 substrate and has overall dimensions of 32.9 × 14.5 × 0.8 mm³. Its geometry is optimised using the Parallel Surrogate-Assisted Differential Evolution Algorithm for Antenna Synthesis (PSADEA). Free-space reflection-coefficient measurements were performed using an Agilent Technologies N5242A vector network analyser. The simulated and measured reflection coefficients are reported below −10 dB over approximately 3–11 GHz, encompassing the conventional 3.1–10.6 GHz UWB allocation. The simulated boresight-gain curve reaches approximately 4.74 dBi. Numerical arm- and breast-phantom models were used to investigate tissue loading; the simulated reflection coefficient remains below −8 dB for the considered antenna-to-phantom separations. The maximum reported 10-g-averaged specific absorption rate (SAR) is approximately 15.85 W/kg at 9.0 GHz for an input power of 1.3 W. A power-scaled estimate at 135 mW is approximately 1.65 W/kg, subject to the assumption of linear scaling. Physical phantom measurements and imaging-level validation were not undertaken; the results therefore establish antenna-level performance rather than diagnostic capability.

Keywords: Biomedical Imaging, Ultra-Wideband Antenna, Antenna Optimisation, Planar Monopole, Tissue Loading

INTRODUCTION

Ultra-wideband (UWB) technology has attracted research interest since the United States Federal Communications Commission authorised unlicensed UWB operation in the 3.1–10.6 GHz band in 2002 (Federal Communications Commission, 2002). Its large operating bandwidth supports short-pulse and broadband sensing applications, including ground-penetrating radar, through-wall sensing, body-centric communications and microwave biomedical imaging. For biomedical imaging, broadband antennas are used to transmit and receive electromagnetic signals whose interaction with tissue depends on the dielectric contrast between different tissue types (Rafique et al., 2022).

Antennas intended for body-centric and biomedical applications must maintain suitable impedance matching and radiation characteristics when positioned near lossy biological tissues. Tissue loading can alter the antenna input impedance, resonant frequencies, radiation pattern and efficiency. These effects make free-space characterisation alone insufficient to describe antenna behaviour in a body-proximity environment (Gabriel & Peyman, 2018; Hall & Hao, 2006). Evaluation under representative tissue-loading conditions is therefore an important stage in assessing candidate antennas for microwave imaging and wearable systems.

Planar monopole antennas are attractive for these applications because they can be compact, low profile and relatively straightforward to fabricate. Slotted radiators provide another design degree of freedom: slots modify current paths and can introduce or shift resonant modes. Previous studies have investigated slotted monopoles for body-centric communication and breast-imaging applications, including Q-slot and T-slot configurations (Celik & Kurt, 2018; Danjuma et al., 2018; Yeboah-Akowuah et al., 2017). The performance of these structures depends on the radiating geometry, feed arrangement and substrate properties, so antenna dimensions and matching must be considered together with tissue-loading behaviour.

Antenna optimisation is also important when several geometrical parameters interact. Surrogate-assisted evolutionary methods combine surrogate modelling with search algorithms to reduce the number of expensive full-wave simulations required during design exploration. The PSADEA approach used in this work combines Gaussian-process surrogate modelling, differential-evolution search and reinforcement-learning-based operator selection; related surrogate-assisted approaches have been described by Akinsolu et al. (2019a, 2019b), Liu et al. (2014, 2017, 2019) and Grout et al. (2019).

Recent work also illustrates the distinction between characterising an antenna and validating a complete biomedical imaging system. For example, a flexible-antenna monitoring vest has been assessed with realistic breast phantoms and compared with anatomical simulation models (Dessai et al., 2024). Such system-level studies include channel measurements and tumour/reference comparisons, whereas the present work is limited to antenna-level free-space measurements and numerical tissue-loading simulations. The proposed design is therefore assessed as an

antenna candidate; the results are not interpreted as evidence of diagnostic performance.

The proposed structure is a compact circular printed monopole with four interconnected T-shaped slots converging at the central region to form a quasi-cross pattern. The antenna is optimised using PSADEA and fabricated on an FR-4 substrate. Experimental characterisation is conducted in free space, while numerical arm- and breast-phantom models are used to examine the reflection coefficient under tissue-loading conditions. SAR is also evaluated numerically for the stated input-power condition.

This study aims to design, optimise, fabricate and experimentally characterise a compact slotted ultra-wideband monopole antenna for biomedical imaging applications under free-space and numerical tissue-loading conditions.

MATERIALS AND METHODS

Proposed Antenna Geometry and Design Parameters

The proposed antenna is a compact planar monopole designed for operation across the conventional UWB band of 3.1–10.6 GHz. The structure is formed on an FR-4 dielectric substrate with relative permittivity εr = 4.3, loss tangent tanδ = 0.025 and thickness 0.8 mm. Its physical dimensions are 32.9 × 14.5 × 0.8 mm³. The radiating element is a circular patch with four interconnected T-shaped slots that converge towards the central region to form a quasi-cross configuration (Figure 1). The antenna is excited by a 50-Ω microstrip feed line defined by its length (ML) and width (MW). The ground structure consists of two identical rectangular conducting sections placed symmetrically on either side of the feed line. The partial-ground dimensions are described by RPL and RPW, while MG denotes the separation between the feed line and the adjacent ground sections. The slot geometry is controlled by the horizontal slot-head dimension (SLH), vertical slot-head dimension (SLV) and slot-throat dimension (SLT). The circular patch dimension is represented by DPR. The figure and original manuscript identify these parameters, but the complete final numerical dimension schedule is not included in the supplied manuscript text; the original design drawing should therefore remain the authoritative geometry record.

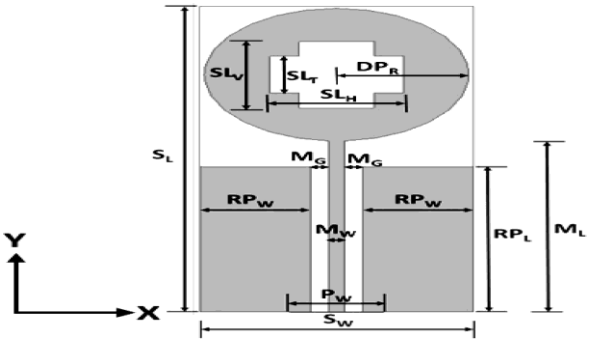

Figure 1: Geometry of The Proposed Circular Monopole Antenna with Four Interconnected T-Shaped Slots and Coplanar Partial-Ground Sections

Numerical Electromagnetic Modelling

The antenna was modelled using CST Microwave Studio. The numerical model included the radiating patch, interconnected T-shaped slots, microstrip feed line, partial ground sections and FR-4 substrate. Simulations were used to evaluate the input reflection coefficient, impedance bandwidth and far-field boresight gain. The operating bandwidth was defined using the −10 dB reflection-coefficient criterion.

The antenna was modelled using CST Studio Suite 2025 with the time-domain finite integration technique (FIT) solver and a hexahedral mesh. The reported maximum mesh density was 20 cells per wavelength, producing approximately 300,000 mesh cells. A single 50-Ω waveguide port was used for excitation. The model included the radiating patch, interconnected T-shaped slots, microstrip feed line, partial-ground sections and FR-4 substrate. The reported convergence criterion was a change of 0.02 dB between successive refinement passes. The specific boundary-condition types and detailed mesh-refinement settings were not available in the study record.

PSADEA-Based Antenna Optimization

The antenna geometry was optimized using the Parallel Surrogate-Assisted Differential Evolution Algorithm for Antenna Synthesis (PSADEA). The approach combines Gaussian-process surrogate modelling with differential-evolution search and reinforcement-learning-based selection of search operators. The surrogate model approximates the electromagnetic response of candidate geometries, while the evolutionary search explores the design space and directs subsequent full-wave evaluations towards promising regions (Akinsolu et al., 2019a, 2019b; Liu et al., 2014, 2017, 2019).

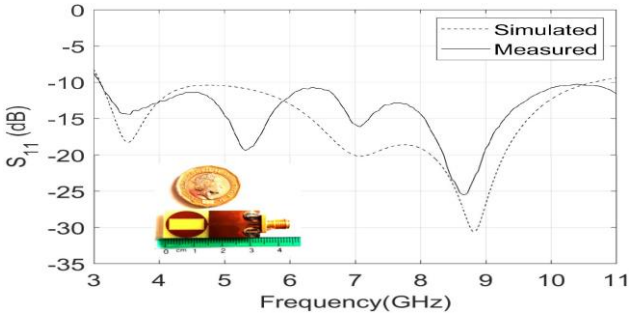

Figure 2: Simulated and Measured Reflection Coefficient (S11) of the Proposed Antenna Under Free-Space Conditions

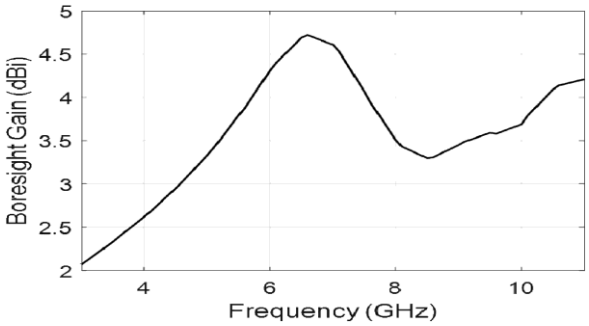

Figure 3: Simulated Boresight Gain of the Proposed Antenna as A Function of Frequency

The optimization variables were DPR, ML, MW, RPL, RPW, MG, SLH, SLV and SLT. The design objective was to obtain suitable impedance matching across 3.1–10.6 GHz while maintaining a compact antenna geometry. The optimization description available for this study does not specify the numerical lower and upper bounds of each variable, the mathematical weighting of the objective function, the initial population size, or the termination criteria. These implementation details are consequently not quantified here. The final geometry was assessed using full-wave electromagnetic simulation.

Fabrication and Experimental Characterization

A physical prototype of the optimized antenna was fabricated on the specified 0.8-mm FR-4 substrate. Free-space reflection-coefficient measurements were performed using an Agilent Technologies N5242A vector network analyzer (VNA). The measured S11 response was compared with the corresponding CST prediction over the reported UWB operating range.

The measurement arrangement used a 50-Ω coaxial RF cable fitted with an SMA male connector. Calibration was performed using the short-open-load-thru (SOLT) method, with the measurement reference plane established at the end of the coaxial cable connected to the antenna's SMA connector. Measurements were conducted in a laboratory free-space environment. The available measurement record does not unambiguously state the exact VNA sweep limits; the plotted results cover approximately 3–11 GHz.

Tissue-Equivalent Phantom Modelling

The influence of biological tissue loading was investigated numerically using separate arm- and breast-phantom models in CST Microwave Studio. The phantom models were not fabricated or measured as physical phantoms; the associated results are therefore numerical evaluations only.

Human Arm Phantom

The arm phantom is a three-layer rectangular structure representing wet skin, fat and muscle, with overall dimensions of 50 mm × 50 mm × 400 mm (Figure 4). At 3.1 GHz, the adopted properties are: wet skin, $\varepsilon_r = 45.85$ and $\sigma = 1.59$ S/m; fat, $\varepsilon_r = 5.28$ and $\sigma = 0.10$ S/m; and muscle, $\varepsilon_r = 52.73$ and $\sigma = 1.74$ S/m. These values are reported at the lower edge of the investigated UWB band. Biological tissue properties are frequency dependent.

The antenna-to-phantom separation was varied from 0 to 15 mm in 5-mm increments, corresponding to separations of 0, 5, 10 and 15 mm. The resulting reflection-coefficient responses were used to examine the sensitivity of the antenna impedance to tissue proximity.

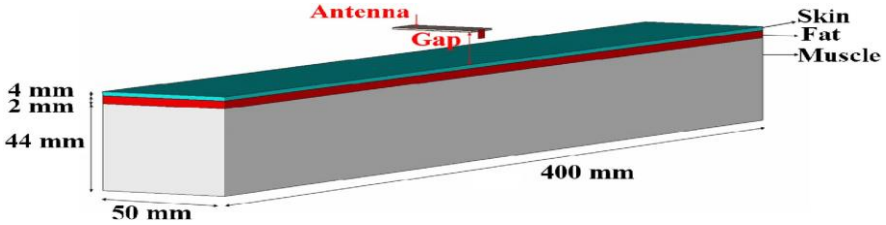

Figure 4: Three-Layer Numerical Arm-Phantom Model Showing the Wet-Skin, Fat and Muscle Regions and The Antenna Separation

Breast Phantom

The breast phantom is represented by a cylindrical tissue-equivalent model with a diameter of 120 mm and an axial length of 150 mm (Figure 5). The model includes plastic covering material with relative permittivity $\varepsilon_r = 1.7$ in place of the muscle layer. The schematic depicts skin and fat regions and a nominal tumour-like inclusion approximately 3–5 mm in diameter. The source description reports a tumour-mimicking mixture comprising 10 g of wheat flour and 5.5 g of water, with relative permittivity $\varepsilon_r = 23$ and conductivity $\sigma = 2.57$ S/m at 4.7 GHz. It also lists a separate set of inclusion properties ($\varepsilon_r = 9$ and $\sigma = 0.4$ S/m), but does not clarify how these values relate to the flour-water mixture. Both arm- and breast-phantom configurations are numerical models; they were not fabricated or experimentally measured.

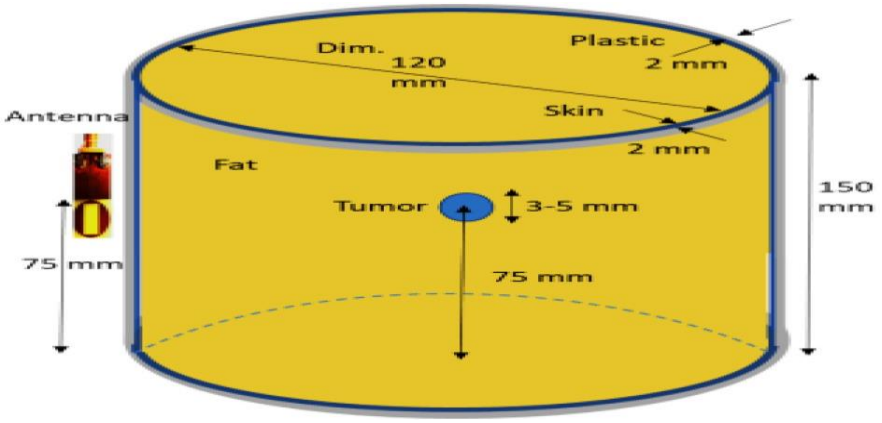

Figure 5: Cylindrical numerical breast-phantom model. The schematic indicates a 120-mm diameter, 150-mm height and a nominal 3–5-mm tumour-like inclusion

Specific Absorption Rate Assessment

Specific absorption rate (SAR) was evaluated numerically to estimate electromagnetic power absorption in the tissue-equivalent model. For an antenna input power of 1.3 W, the reported maximum 10-g-averaged SAR was approximately 15.85 W/kg at 9.0 GHz. Assuming that the electromagnetic field distribution remains unchanged and SAR scales linearly with input power, the corresponding estimate at 135 mW is $15.85 \times (0.135/1.3) \approx 1.65$ W/kg, averaged over 10 g. This is a power-scaled estimate rather than a separately simulated SAR result. Compliance with an exposure standard cannot be inferred without confirming the applicable jurisdiction, averaging mass, exposure conditions and the corresponding SAR result under the required assessment procedure.

Under a linear power-scaling assumption and with the same field distribution and phantom model, the corresponding estimate is $15.85 \times (0.135/1.3) \approx 1.65$ W/kg averaged over 10 g.

RESULTS AND DISCUSSION

Free-Space Reflection Coefficient

Figure 2 compares the simulated and measured reflection coefficients of the fabricated antenna under free-space conditions. The reported reflection coefficient remains below −10 dB over an approximate 3–11 GHz range, encompassing the conventional UWB allocation of 3.1–10.6 GHz. Agreement between the simulated and measured responses is reported up to approximately 10.8 GHz. Differences are most evident around the second resonance, where the measured response is broader and less pronounced than the simulated response.

Consequently, the agreement is described qualitatively rather than assigned an unsupported numerical error. The observed deviations may be associated with substrate-property variation, fabrication tolerances and uncertainties in the measurement connection and calibration.

Boresight Gain

The boresight-gain response is shown in Figure 3. The plotted curve reaches a maximum of approximately 4.74 dBi near 6.7 GHz. The figure caption identifies this result as simulated boresight gain; accordingly, it is reported here as a simulated value and not as an experimentally measured gain.

Antenna Response Under Tissue Loading

Figures 4 and 5 show the arm- and breast-phantom geometries used in the numerical investigation. Figure 6 presents the simulated S11 responses for the antenna at different distances from the arm phantom: direct contact and separations of 5, 10 and 15 mm. The reported S11 remains below −8 dB over the investigated frequency range, with comparatively small changes as the separation varies.

The phantom results indicate that the antenna maintains a degree of impedance stability under the modelled tissue-loading conditions.

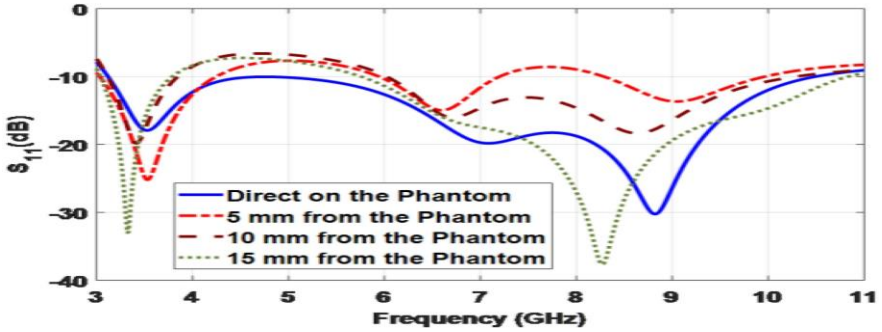

Figure 6: Simulated Reflection Coefficient (S11) For The Antenna at Direct Contact and at 5, 10 And 15 Mm from The Arm Phantom.

SAR Results and Exposure Considerations

For the 1.3 W input-power condition, the reported maximum SAR averaged over 10 g of tissue is approximately 15.85 W/kg at 9.0 GHz. Linear scaling to an input power of 135 mW gives an estimated 10-g-averaged SAR of approximately 1.65 W/kg. This estimate assumes an unchanged field distribution and should not be treated as a substitute for a new SAR simulation. In addition, SAR limits depend on the applicable regulatory framework and averaging mass; a 10-g result cannot be used to establish compliance with a 1-g limit. The

present numerical result therefore indicates the need for a complete SAR assessment at the intended operating power before practical deployment.

Table 1: Comparison of The Proposed Antenna with Selected UWB Antennas for Biomedical and Body-Centric Applications

Antenna	Overall dimensions (mm^3)	−10 dB operating band	Gain / directivity	Radiation efficiency	Substrate and validation
Yeboah-Akowuah et al. (2017), Q-slot monopole	36.6 × 39 × 1.6	3.5–11.7 GHz (S11 < −10 dB)	Realised gain: 4.33, 4.90 and 6.00 dB at 3.5, 6.5 and 9 GHz	98.40%, 99.60%, 98.68% at 3.5, 6.5, 9 GHz	FR-4; εr = 3, tanδ = 0.01; measured free-space and on-body/phantom response
Celik and Kurt (2018), directive disc monopole	Not reported	3–10 GHz; 108% reported bandwidth	Directivity: 6.2–9.4 dBi (not gain)	Not reported	HFSS design and VNA test; breast-imaging application
Danjuma et al. (2018), T-slot circular monopole	Not reported	3.1–10.6 GHz	Gain evaluated; numeric maximum Not reported in abstract	Efficiency evaluated; numeric values Not reported	Simulation and measurement of impedance, gain, pattern and efficiency
Proposed slotted monopole	32.9 × 14.5 × 0.8	Approximately 3–11 GHz; includes 3.1–10.6 GHz	Maximum simulated boresight gain ≈ 4.74 dBi	Not reported	FR-4; εr = 4.3, tanδ = 0.025; free-space S11 measured; arm/breast loading simulated only

The comparison shows that compact dimensions alone do not establish superior performance. The Q-slot antenna reported by Yeboah-Akowuah et al. (2017) provides measured and calculated characterisation in free space and on-body conditions, together with numerical gain and efficiency values. Celik and Kurt (2018) reported a 3–10 GHz operating band and directivity between 6.2 and 9.4 dBi for a directive antenna intended for breast-imaging radar. Danjuma et al. (2018) also reported a T-slot circular monopole evaluated over 3.1–10.6 GHz, including simulated and measured impedance, gain, radiation pattern and efficiency. These studies provide broader radiation and tissue-related evaluation than can be established from the present source data. Recent system-level work using realistic breast phantoms further demonstrates the importance of tumour/reference measurements and imaging-level validation (Dessai et al., 2024). The present contribution is therefore the compact PSADEA-optimised geometry and its free-space S11 characterisation, together with preliminary numerical tissue-loading and SAR assessment; diagnostic performance has not been demonstrated.

CONCLUSION

This study has presented the design, PSADEA-based optimisation, fabrication and experimental free-space characterisation of a compact slotted UWB monopole antenna for potential biomedical imaging applications. The antenna comprises a circular radiating patch with four interconnected T-shaped slots and is fabricated on a 0.8-mm FR-4 substrate with overall dimensions of 32.9 × 14.5 × 0.8 mm^3. The simulated and measured reflection coefficients are reported below −10 dB over approximately 3–11 GHz, covering the conventional 3.1–10.6 GHz UWB band, while the simulated boresight gain reaches approximately 4.74 dBi. Numerical arm- and breast-phantom models were used to investigate tissue loading, and the simulated reflection coefficient remained below −8 dB for the considered antenna-to-arm-phantom separations. The reported maximum 10-g-averaged SAR was approximately 15.85 W/kg at 9.0 GHz for 1.3 W input power; linear power scaling gives an estimate of approximately 1.65 W/kg at 135 mW, which requires confirmation by a separate SAR simulation. The principal contribution is the compact PSADEA-optimised antenna and its free-space impedance characterisation, supported by numerical tissue-loading analysis. The study does not demonstrate experimental phantom measurements, image reconstruction, tumour detection or diagnostic accuracy. Further work should provide complete optimisation and simulation settings, validate the antenna using characterised physical tissue phantoms, quantify measurement uncertainty, perform SAR assessment under the applicable exposure standard and evaluate the antenna within a complete microwave-imaging system.

REFERENCES

Akinsolu, M. O., Danjuma, I. M., Mistry, K. K., Liu, B., Abd-Alhameed, R. A., Lazaridis, P. I., Zaharis, Z. D., & Excell, P. (2019a). Efficient AI-driven design of microwave antennas using PSADEA. *In Proceedings of the 2nd IEEE Middle East and North Africa Communications Conference (MENACOMM)* (pp. 1–5). https://doi.org/10.1109/MENACOMM46666.2019.8988550

Akinsolu, M. O., Liu, B., Grout, V., Lazaridis, P. I., Mognaschi, M. E., & Di Barba, P. (2019b). A parallel surrogate model assisted evolutionary algorithm for electromagnetic design optimization. *IEEE Transactions on Emerging Topics in Computational Intelligence, 3*(2), 93–105. https://doi.org/10.1109/TETCI.2018.2864747

Celik, A. R., & Kurt, M. B. (2018). Development of an ultra-wideband, stable and high-directive monopole disc antenna for radar-based microwave imaging of breast cancer. *Journal of Microwave Power and Electromagnetic Energy, 52*(2), 75–93. https://doi.org/10.1080/08327823.2018.1458692

Danjuma, I. M., Akinsolu, M. O., Oguntala, G., Asahraa, A., Abd-Alhameed, R. A., Bin-Melha, M., Elfergani, I. T. E., Rodriguez, J., & Liu, B. (2018). A T-slot monopole antenna for UWB microwave imaging applications. In *Proceedings of*

the Loughborough Antennas & Propagation Conference (LAPC 2018). https://doi.org/10.1049/cp.2018.1491

Dessai, R., Singh, D., Sonkki, M., Reponen, J., Myllylä, T., Myllymäki, S., & Särestöniemi, M. (2024). A breast tumor monitoring vest with flexible UWB antennas—A proof-of-concept study using realistic breast phantoms. *Micromachines, 15*(9), Article 1153. https://doi.org/10.3390/mi15091153

Federal Communications Commission. (2002). Revision of Part 15 of the Commission's rules regarding ultra-wideband transmission systems: First report and order (FCC 02-48). https://docs.fcc.gov/public/attachments/FCC-02-48A1.pdf

Gabriel, C., & Peyman, A. (2018). Electric and magnetic properties of biological materials. In *Bioengineering and biophysical aspects of electromagnetic fields* (4th ed., pp. 101–159). https://doi.org/CRC-Press

Grout, V., Akinsolu, M. O., Liu, B., Lazaridis, P. I., Mistry, K. K., & Zaharis, Z. D. (2019). Software solutions for antenna design exploration: A comparison of packages, tools, techniques, and algorithms for various design challenges. *IEEE Antennas and Propagation Magazine, 61*(3), 48–59. https://doi.org/10.1109/MAP.2019.2907887

Hall, P. S. (2007). Antennas challenges for body-centric communications. In *Proceedings of the International Workshop on Antenna Technology: Small Smart Antennas, Metamaterials and Applications* (pp. 41–44).

Hall, P. S., & Hao, Y. (2006). Antennas and propagation for body-centric communications. In *Proceedings of the 2006 First European Conference on Antennas and Propagation* (pp. 1–7).

Liu, B., Akinsolu, M. O., Ali, N., & Abd-Alhameed, R. A. (2019). Efficient global optimisation of microwave antennas based on a parallel surrogate model-assisted evolutionary algorithm. *IET Microwaves, Antennas & Propagation, 13*(2), 149–155. https://doi.org/10.1049/iet-map.2018.5009

Liu, B., Koziel, S., & Ali, N. (2017). SADEA-II: A generalized method for efficient global optimization of antenna design. *Journal of Computational Design and Engineering, 4*(2), 86–97. https://doi.org/10.1016/j.jcde.2016.11.002

Liu, B., Zhang, Q., & Gielen, G. G. (2014). A Gaussian process surrogate model assisted evolutionary algorithm for medium scale expensive optimization problems. *IEEE Transactions on Evolutionary Computation, 18*(2), 180–192. https://doi.org/10.1109/TEVC.2013.2248012

Rafique, U., Pisa, S., Cicchetti, R., Testa, O., & Cavagnaro, M. (2022). Ultra-wideband antennas for biomedical imaging applications: A survey. *Sensors, 22*(9), Article 3230. https://doi.org/10.3390/s22093230

Yeboah-Akowuah, B., Kosmas, P., & Chen, Y. (2017). A Q-slot monopole for UWB body-centric wireless communications. *IEEE Transactions on Antennas and Propagation, 65*(10), 5069–5075. https://doi.org/10.1109/TAP.2017.2740977

©2026 This is an Open Access article distributed under the terms of the Creative Commons Attribution 4.0 International license viewed via https://creativecommons.org/licenses/by/4.0/ which permits unrestricted use, distribution, and reproduction in any medium, provided the original work is cited appropriately.